

# Analysis of Keck HIRES spectra of early L-type dwarfs

Andreas Schweitzer

*Department of Physics and Astronomy & Center for Simulational Physics, University of Georgia, Athens, GA 30602-2451*

andy@physast.uga.edu

John E. Gizis

*Infrared Processing and Analysis Center, 100-22, California Institute of Technology, Pasadena, CA 91125*

gizis@ipac.caltech.edu

Peter H. Hauschildt

*Department of Physics and Astronomy & Center for Simulational Physics, University of Georgia, Athens, GA 30602-2451*

yeti@hobbes.physast.uga.edu

France Allard

*CRAL, Ecole Normale Supérieure, 46 Alle d'Italie, Lyon, 69364, France*

fallard@ens-lyon.fr

and

I. Neill Reid

*Department of Physics and Astronomy, University of Pennsylvania, 209 South 33rd Street, Philadelphia PA 19104-6396*

inr@hep.upenn.edu

## ABSTRACT

We present analyses of high resolution and medium resolution spectra of early L dwarfs. We used our latest set of model atmospheres to reproduce and analyze the observed features. We can model the optical flux and the atomic line profiles with the best accuracy to date. The models used to reproduce the observations

include dust condensation and dust opacities. Compared to previous studies using older models we find that our dust treatment is much improved. The derived parameters for the objects are well in the expected range for old very low mass objects. This is also supported by the absence of Li in most of the objects. For the objects showing Li we can be almost certain that those are brown dwarfs. However, a spectral analysis in general, and this one in particular can only very roughly determine mass and age.

*Subject headings:* stars: low-mass, brown dwarfs – line: profiles – stars: atmospheres – stars: fundamental parameters

## 1. Introduction

In recent years many new very low mass objects have been discovered, classified and the techniques to detect and observe them have been refined. With the increased sample size has come the discovery of bright sources, whose characteristics can be assumed to be representative of the underlying population. Those bright sources are accessible to study at high resolution and high signal-to-noise. Such investigations can now enable us to measure their parameters which is necessary if we want to understand the physics and nature of very low mass objects in general.

The models for such objects have experienced an equally rapid evolution in the last few years. The latest model atmospheres incorporate the presence of dust within the atmosphere. Although it has become clear that dust does form in cool atmospheres a realistic reproduction of the observed effects has not been achieved yet. The problems associated with implementing an accurate treatment of dust in cool dwarf atmospheres include devising consistent formation and destruction mechanisms, including condensation and diffusion, besides incorporating a realistic treatment of opacities.

Earlier work on the interpretation of L dwarf spectra (e.g. Burrows et al. 2000; Pavlenko et al. 2000; Leinert et al. 2000) focused either on the reproduction and explanation of individual features or used medium to low resolution spectra. Basri et al. (2000) analyzed high resolution spectra of a sample of L dwarfs using a first generation of the dusty and rained out models by Allard et al. (1997). The dusty models used in this earlier work seemed to overestimate the effects of the dust on the optical line formation. The rained out models appeared to provide an adequate fit to the lines. However, it was clear from other work by Ruiz et al. (1997), Leggett et al. (1998), and Kirkpatrick et al. (1999a) that these L type dwarfs share the near-infrared properties of dusty models and not those of rained out models.

Recently, Allard et al. (2001) computed an improved set of dusty and rained out models which include revised opacity and dust treatment. These models were used by Leggett et al. (2001) to analyse low and medium resolution spectra of the overall spectral distribution of M and L dwarfs. Their results confirmed that the new models could still reproduce the near-infrared properties of L dwarfs within uncertainties of the water vapor opacity profile, but also showed that they fitted adequately their optical spectral distributions.

In this paper we will use the improved models of Allard et al. (2001) which were also used in Leggett et al. (2001) to perform analyses of optical high resolution spectra similarly to Basri et al. (2000). In the next section we will describe the available data, in Section 3 we will describe the models and the important improvements, Section 4 contains the methods we used to analyze the data and the results.

## 2. Observations and data

Echelle spectroscopy of the L dwarfs discussed in this paper was obtained using the HIRES spectrograph (Vogt et al. 1994) on the Keck I 10-meter telescope. The observations were made on 23 and 24 August 1998, 13 November 1998 and 6 and 7 June 1999. In each case we used the red cross-disperser, covering selected regions of the spectrum in the 6000 to 9800Å wavelength region. The August observations were made using the  $1''.15 \times 7''.0$  slit, giving a resolution of  $\sim 34,000$  ( $8.8 \text{ kms}^{-1}$  or 4 pixels); seeing was sufficiently better than 1 arcsecond on the other three nights to allow use of the  $0''.86 \times 7''.0$  slit, giving an increased resolution of  $\sim 45,000$  ( $6.4 \text{ kms}^{-1}$  or 3 pixels). Typical exposure times were 3000 seconds.

The echelle data were extracted using the *mckee* suite of programs, written by T. Barlow. Most of the L dwarfs are barely detected at wavelengths shortward of  $\sim 7000\text{\AA}$  (sometimes  $\lambda < 8000\text{\AA}$ ), so we used observations of brighter, near-featureless stars (usually white dwarfs) as templates to outline the shape of each order. Similar techniques were used to extract the thorium-argon wavelength calibration spectra, obtained at the start and end of each night, while flat-field images are used to correct gross non-uniformities. The data were wavelength calibrated using standard IRAF routines and the thorium-argon spectra. We have not attempted to set the spectra on an absolute flux scale.

The low resolution spectra are data published in Kirkpatrick et al. (1999b) and Kirkpatrick et al. (2000).

### 3. The models

The models used in this work are the ones described in Allard et al. (2001). A detailed description can be found therein. They are the same as in the earlier work of Leggett et al. (2001). The models utilize the Ames H<sub>2</sub>O and TiO line lists by Partridge & Schwenke (1997) and Schwenke (1998). We stress that large uncertainties persist in these line data for the temperature range of this work (see Allard et al. 2000). The opacities in the models have been upgraded with (i) the replacement of the JOLA (Just Overlapping Line Approximation) opacities for FeH, VO and CrH by theoretical line data for which we do dynamical opacity sampling as described in Allard et al. (2001), (ii) the extension of our database of dust grain opacities from 10 to 40 species which are based on laboratory measurements and (iii) the revision of pressure induced H<sub>2</sub> opacities.

The dust for all the species of Sharp & Huebner (1990) forms in chemical equilibrium using the Gibbs free energy from the JANAF database (Chase et al. 1985). The models treat the dust in the limiting case where the dust is in equilibrium with the gas phase. When dust forms in a layer it does not diffuse out of the layer but contributes in full to the opacity (Ames-Dusty-2000 models). As comparison we also used the other extreme where the dust forms and completely settles below the atmosphere (Ames-Cond models) and, therefore, does no longer contribute to the opacity. A detailed description of the treatment of dust and of the effects of dust on the temperature structure and the spectrum can be found in Allard et al. (2001).

The temperature structures of these models were used to calculate synthetic high resolution spectra at a resolution of 0.1Å between 6400 and 9100Å for all the models used in this analysis. The atomic lines in the spectra are dominated by van der Waals pressure broadening which has been taken into account as in the calculations as described in Schweitzer et al. (1996). Although not part of the targeted wavelength range, our calculations naturally include all strong lines whose wings end up in the targeted wavelength range (see e.g. Hauschildt et al. 1999). This includes most prominently the wings of the very strong Na D doublet. For the fitting process, the spectra were rotationally broadened if necessary. They were then convolved with a Gaussian to match the resolution of the observed HIRES spectra.

We include van der Waals (vdW) broadening since the lines are pressure broadened due to collisions with neutral species. We use a modification of the Unsöld treatment of vdW broadening which considers not only H but also H<sub>2</sub>, He and the most abundant trace species (see Schweitzer et al. 1996). In a different study, Burrows et al. (2000) deploy an approximation for pressure broadening due to H<sub>2</sub> which is an extension to the impact approximation used by the Unsöld approach. For our model structures we calculated the Weisskopf radius which distinguishes between the validity of the impact theory and the

statistical theory of vdW broadening (see Burrows et al. 2000) but found that the impact theory is adequate. This was confirmed by other tests we have made using different line broadening profiles like Margenau profiles (Margenau 1932), which is a general approach to the statistical theory and proved worse (see section 4.2 for the high resolution fits). However, the models presented by Burrows et al. (2000) (which do not use a plain Unsöld treatment) do not include the molecular line data present in our models and, as a result, predict substantially different spectral energy distributions. Both sets of models therefore have their limitations. We aim to integrate more sophisticated broadening calculations, especially for the treatment of the far wings of resonance lines, in a future generation of stellar models.

However, the most important impact on line profiles is caused by the presence of dust. This has already been demonstrated and investigated by Leinert et al. (2000) and Basri et al. (2000) where Dusty and Cond models have been compared in reproducing individual lines. The line width is very sensitive to the amount of dust as a function of layer. Errors on line broadening theories become negligible compared to the effect of dust and that justifies why the former should only be addressed once the dust issue is settled.

## 4. Analysis and results

We used a  $\chi^2$  fitting technique to determine the best fitting model spectra. We used a grid of model spectra and for each spectrum we calculated a  $\chi^2$  in order to determine the best fitting model which had the smallest  $\chi^2$ . All spectra were visually inspected. Some fits had to be corrected when the best fitting model was a feature poor spectrum and the fit was simply an overall canceling out of the observed features in the  $\chi^2$  determination. Excluding the problematic model from the grid of theoretical models usually corrected this problem. We did this for fitting both the low resolution models and the high resolution models. Our grid of theoretical spectra consisted of solar metallicity models with effective temperatures between 1600 K and 2400 K in steps of 100 K and surface gravities with  $\log(g)$  between 3.5 and 5.5 in steps of 0.5.

### 4.1. Results for the low resolution spectra

We used the low resolution spectra to determine a first fit of the effective temperature. We compared the effect of  $\log(g)$  for constant effective temperature and found that the gravity does not significantly change the shape of the optical low-resolution spectra. This

is also supported by the results of our  $\chi^2$  fitting techniques which finds similar effective temperatures rather than similar gravities as the three best fitting models. We restricted the wavelength range to 7700Å to 9900Å to avoid the problematic VO band on the blue side of the wavelength range and the problematic FeH band on the red side. For both of these bands we use the latest not fully tested available data.

The results of the fitting process is summarized in Tab. 1 The derived parameters have a determination uncertainty of 100 K in effective temperature and 0.5 dex in  $\log(g)$ . These errors reflect the spacing of the grid. The  $\chi^2$  fitting process also determines the second and third best fits within 100 K and 0.5 dex. These errors do not include any systematic problems in the models and the values have to be considered as determined within the used models. The table lists the fits for both the AMES-Dusty and the AMES-Cond models. Except for the L3.5 dwarf, the Dusty models give better fits when inspected visually. With the AMES-Cond models the K I is too strong and the CrH and FeH bands at 8611Å and 8692Å are too strong. This is still the case for the L3.5 dwarf, however, for all parameters, the K I doublet is too weak. This gives a hint that at these temperatures models between the limiting cases of AMES-Dusty and AMES-Cond start being more appropriate. Such models that calculate the amount of dust which diffuses are being developed (Allard et al., in preparation). They will be needed for effective temperatures below approximately 1800 K. In this paper the dwarfs are reasonably hot enough that such models are not required. The fact that we can use the limiting AMES-Dusty models is also supported by the results of Leggett et al. (2001); and Chabrier et al. (2000) suggests that such atmosphere conditions exist.

The fits to the low resolution spectra usually return high gravity values. This is because the high gravity spectra have very broad atomic lines which smooth the whole spectrum. These spectra are therefore preferred by the  $\chi^2$  test.

The fits of AMES-Dusty models to the low resolution spectra are shown in Figs. 1 through 5. As can be seen the molecular bands are well reproduced. This is true for VO, CrH and FeH which produce the various features and also for TiO which determines the overall optical spectrum. No attempt has been made to fit individual strong atomic lines like the K I resonance doublet or the Na I subordinate doublet. The purpose of these fits was to determine the effective temperature by fitting the overall shape which is dominated by molecular absorption. The region around the Na I doublet usually can be fit by scaling the spectra but this would worsen the fit elsewhere. Similarly for the K I doublet, which could be fit better by slightly different parameters. This problem will be addressed below when discussing the differences between the results from high resolution and low resolution spectra.

As expected and within the error bars our fits confirm a correlation of spectral type with effective temperature. The overall temperature range of only 300 K for 4 spectral classes is not that small when translating the effective temperature back into luminosity (which it originally defines). However, the small temperature range is also not very surprising since dust condensation (and the associated molecule depletion) takes place very rapidly in parameter space. Therefore, molecular features are very sensitive to changes in  $T_{\text{eff}}$ .

#### 4.2. Results for the high resolution spectra

We fitted model spectra to the Cs I line at 8521.36 Å, the Rb I lines at 7800.26 Å and 7947.60 Å, the Na I doublet at 8190 Å and the K I at 7685 Å doublet when these lines were in the observed wavelength range. For two spectra we also used the Ca I line at 6572.77 Å and for one we used the Li I line at 6707.76 Å. The results are tabulated in Tab. 2. The table also demonstrates which lines could be observed in which object. The fits to the lines are shown in Figs. 6–14.

As can be seen the derived temperatures do not correlate with spectral type and the temperature derived from the low resolution spectra. The error bars are again 100 K and 0.5 dex within the previously established limits. The derived temperatures from low resolution and high resolution spectra don not agree for the later dwarfs in the sample. Only the earlier type objects show a weak correlation between effective temperatures derived from low resolution and high resolution spectra. To prevent a discrepancy between low resolution and high resolution spectra we could have fixed the effective temperature to the one derived from the low resolution spectra during the fitting process. We attempted this but the resulting fits were very poor so that we left the effective temperature as a free parameter.

The reason for the discrepancy between effective temperatures derived from low resolution spectra and high resolution spectra is most likely a dust opacity and dust settling problem (see also Leinert et al. 2000). A combination of temperature structure and opacity structure produces a line that “looks” too hot for the later dwarfs. This is another indicator that the cooler the models get, the less satisfied the conditions are that allow the use of the AMES-Dusty models. Usage of more consistent models will first change only parts of the atmosphere before the whole atmosphere and spectrum changes. The molecular bands form in different regions and will be affected differently by partial incorrectness than atomic lines which usually form in the deepest layers.

For each object, the values of  $\log(g)$  are usually within  $\pm 0.5$  dex. However, all objects have rather large values for  $\log(g)$  although the used parameter range started as low as

$\log(g)=3.5$ . This means that all objects have already contracted considerably. This is also supported by the fact that only two objects show the Li I line. We discuss this in detail in section 4.4.

All the models had been rotationally broadened if necessary. We did not include the rotationally velocity in the automatic fitting process. We rather adjusted this parameter by visual inspection. We want to note, however, that changing the rotational velocity by 5 or 10  $\text{km s}^{-1}$  did usually change the quality of the fit, but it did not change the parameters of the best fitting models. Therefore, the accuracy of the rotational broadening is not important for the determination of  $T_{\text{eff}}$  and  $\log(g)$ . Keeping these caveats in mind we give the best fitting values for the rotational velocity in Tab. 2.

### 4.3. 2MASS0345+2540

2MASS0345+2540 was also in the sample of Leggett et al. (2001) who found  $T_{\text{eff}}=2000$  K and  $\log(g)=6.0$ , whereas we find  $T_{\text{eff}}=1900$  K and  $\log(g)=5.5$ . This is well consistent within the error bars. It is however to note that Leggett et al. (2001) used the full spectral range from the optical to the NIR. The current data for water still has uncertainties (Allard et al. 2000) as it does not reproduce the H-band correctly. This affects the overall flux distribution and the optical will have a different pseudo-continuum level. An unrealistically shaped overall spectrum will also affect the pure technical fitting process which will find the best compromise. Both these effects will lead to systematic differences between this work and the work of Leggett et al. (2001).

This example shows that there is an unknown systematic error in addition to the the error bars from our measurement. Using a larger wavelength range and using better line opacities (which is not possible at the moment) may change the results.

### 4.4. Li presence and substellar nature

We only derived high ( $\gtrsim 4.5$ ) values for  $\log(g)$ . This is consistent with the fact that only the two objects 2MASS1146+2230 and 2MASS1726+1538 show a Li I line. The Li I line in 2MASS1726+1538 is very weak (see Kirkpatrick et al. 2000) and is not detected in the HIRES observation. To demonstrate this consistency we plot  $T_{\text{eff}}$  versus  $\log(g)$  from the data by Chabrier et al. (2000) in Fig. 15. The dotted lines indicate 95% Li abundance remaining (left line) and 50% Li abundance remaining (right line). As can be seen, objects without Li should all have  $\log(g)$  above 5.0, which is what we derived. 2MASS1146+2230 will then have



to have a  $\log(g)$  in the lower part of its error bars and is almost certainly a brown dwarf. 2MASS1726+1538 has a very weak Li I line and is, therefore, in the strip where Lithium depletion occurs. In the context of these models, 2MASS1726+1538 then has  $\log(g)=5.25$  and  $m \approx 0.06 m_{\odot}$  and would be a brown dwarf as well. All other objects are hot enough to be either brown dwarfs or stars. The tracks below  $\log(g)=4.5$  correspond to masses below  $0.03 M_{\odot}$  and ages significantly younger than 100 Myrs. Such objects are unlikely to be found in a field sample such as 2MASS.

We want to emphasize that the derived error bars are much too large to use the spectroscopic parameters to determine mass and age from such a diagram. We use this diagram for illustrative purposes and to show that we are consistent with what is expected from evolutionary models.

## 5. Discussion and summary

We have presented fits to high and medium resolution spectra of L dwarfs using our latest model atmospheres and synthetic spectra.

The observed spectra including the high resolution line profiles can be reproduced very well. The derived parameters from the best fitting models are physically reasonable. They match the expected parameters for old ( $\gtrsim 1\text{Gyr}$ ) VLM stars and massive brown dwarfs.

The important physics in the models is the inclusion of dust condensation and dust opacity as described above. The models used in this analysis use the limiting case in which the dust forms and does not diffuse. Since most objects can be well reproduced with these models, this assumption seems to be well justified for early L dwarfs. However, we found hints that for objects later than L3 (or with our models cooler than 1800 K) the assumption for the limiting case is no longer fully met (see also Leggett et al. 2001).

Most importantly, however, within the valid range our models reproduce accurately the observed spectra. Our new models reproduce realistic line profiles in the presence of dust. The applied Unsöld treatment for the vdW broadening is only an approximation. But for the objects in this paper it reproduces the atomic lines very well within the limits of the dust distribution uncertainties. Tests using other profiles did not reproduce better profiles. We are actively improving the models and considering more realistic line broadening mechanism similar to Burrows et al. (2000) but find no reason to change the current implementation yet.

We encountered the problem that the determined effective temperatures from high res-

olution spectra are different than those from low resolution spectra. We think this could have two reasons. The first one could be that the line formation of the atomic lines is not reproduced correctly due to an incorrect temperature or opacity structure. This can easily happen if the dust treatment does not produce the right dust properties for all layers (see also Leinert et al. 2000). The second reason is simply the fact that the pseudo continuum level in the optical is probably not correct due to incorrect or incomplete line data. If the molecular line data is incorrect then the overall flux is not distributed correctly which will lead to different pseudo continuum around the atomic lines and thus different best fitting parameters for atomic lines.

Both of these effects can be interpreted as seeing hotter (or cooler) temperatures in the atomic lines. Therefore, we think that the distortions on the  $\log(g)$  determinations are not very large and that our derived  $\log(g)$  values are not affected very much. This is also supported by the fact that we find high values for  $\log(g)$  for objects without Li (see above).

Future models, which are being developed, will include a more consistent dust treatment which will also be valid for lower temperatures and later L dwarfs. The improved dust treatment plus more complete and improved line data which becomes available over time will make the models applicable to early and late type L dwarfs at the same time and it will give consistent results for low resolution and high resolution spectra.

We are grateful to Richard Freedman (NASA-Ames) who generously provided VO and CrH line lists for use in the current models. AS acknowledges support from NASA ATP grant NAG 5-8425 to the University of Georgia. JEG acknowledges the support of the Jet Propulsion Laboratory, California Institute of Technology, which is operated under contract with NASA. PHH acknowledges support in part from NASA ATP grant NAG 5-3018 and LTSA grant NAG 5-3619 to the University of Georgia and partial support from the Pôle Scientifique de Modélisation Numérique at ENS-Lyon. FA acknowledges support from CNRS. INR acknowledges partial support from a NASA/JPL grant to 2MASS Core Project Science. This work was also supported in part by NSF grants AST-9417242, AST-9731450, and NASA grant NAG5-3505 and an IBM SUR grant to the University of Oklahoma. Some of the calculations presented in this paper were performed on the IBM SP and the SGI Origin 2000 of the UGA UCNS, on the IBM SP of the San Diego Supercomputer Center (SDSC, with support from the National Science Foundation), on the Cray T3E and the IBM SP of the NERSC with support from the DoE, on the IBM SP2 of the French Centre National Universitaire Sud de Calcul (CNUSC). We thank all these institutions for a generous allocation of computer time. This paper is partially based on observations obtained at the W. M. Keck Observatory, which is operated jointly by the University of California, the California Institute of Technology and NASA.

## REFERENCES

- Allard, F., Hauschildt, P. H., Alexander, D. R., Tamanai, A., & Schweitzer, A. 2001, *ApJ*, submitted
- Allard, F., Hauschildt, P. H., Alexander, D. R., & Starrfield, S. 1997, *ARA&A*, 35, 137
- Allard, F., Hauschildt, P. H., & Schwenke, D. 2000, *ApJ*, 540, 1005
- Basri, G., Mohanty, S., Allard, F., Hauschildt, P. H., Delfosse, X., Martín, E. L., Forveille, T., & Goldman, B. 2000, *ApJ*, 538, 363
- Burrows, A., Marley, M. S., & Sharp, C. M. 2000, *ApJ*, 531, 438
- Chabrier, G., Baraffe, I., Allard, F., & Hauschildt, P. H. 2000, *ApJ*, 542, in press
- Chase, M. W., Davis, C. A., Downey, J. R., Frurip, D. J., McDonald, R. A., & Syverud, A. N. 1985, *J. Phys. Chem. Ref. Data*, 14, Sup.1
- Hauschildt, P. H., Allard, F., & Baron, E. 1999, *ApJ*, 512, 377
- Kirkpatrick, J. D., Allard, F., Bida, T., Zuckerman, B., Becklin, E. E., Chabrier, G., & Baraffe, I. 1999a, *ApJ*, 519, 834
- Kirkpatrick, J. D., Reid, I. N., Liebert, J., Cutri, R. M., Nelson, B., Beichman, C. A., Dahn, C. C., Monet, D. G., Gizis, J. E., & Skrutskie, M. F. 1999b, *ApJ*, 519, 802
- Kirkpatrick, J. D., Reid, I. N., Liebert, J., Gizis, J. E., Burgasser, A. J., Monet, D. G., Dahn, C. C., Nelson, B., & Williams, R. J. 2000, *AJ*, 120, 447
- Leggett, S., Allard, F., Geballe, T., Hauschildt, P., & Schweitzer, A. 2001, *ApJ*, in press
- Leggett, S. K., Allard, F., & Hauschildt, P. H. 1998, *ApJ*, 509, 836
- Leinert, C., Allard, F., Richichi, A., & Hauschildt, P. H. 2000, *A&A*, 353, 691
- Margenau, H. 1932, *Physical Review*, 40, 387
- Partridge, H. & Schwenke, D. W. 1997, *J. Chem. Phys.*, 106, 4618
- Pavlenko, Y., Zapatero Osorio, M. R., & Rebolo, R. 2000, *A&A*, 355, 245
- Ruiz, M. T., Leggett, S. K., & Allard, F. 1997, *ApJ*, 491, L107
- Schweitzer, A., Hauschildt, P. H., Allard, F., & Basri, G. 1996, *MNRAS*, 283, 821

Schwenke, D. W. 1998, *Faraday Discussions*, 109, 321

Sharp, C. M. & Huebner, W. F. 1990, *ApJS*, 72, 417

Vogt, S. S., Allen, S. L., Bigelow, B. C., Bresee, L., Brown, B., Cantrall, T., Conrad, A., Couture, M., Delaney, C., Epps, H. W., Hilyard, D., Hilyard, D. F., Horn, E., Jern, N., Kanto, D., Keane, M. J., Kibrick, R. I., Lewis, J. W., Osborne, J., Pardeilhan, G. H., Pfister, T., Ricketts, T., Robinson, L. B., Stover, R. J., Tucker, D., Ward, J., & Wei, M. Z. 1994, *Proc. SPIE*, 2198, 362

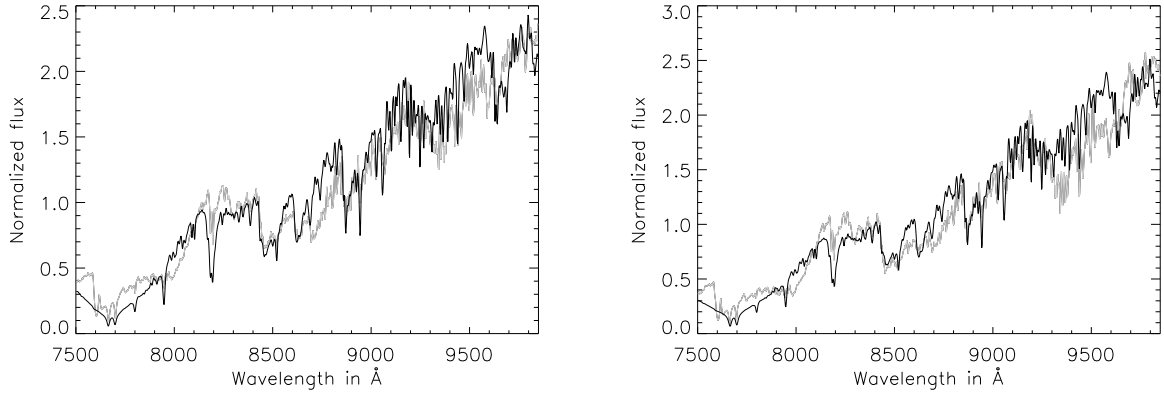


Fig. 1.— Fits (dark line) to the observed dwarfs (grey line) to 2M0149+2956 (left panel) and 2M2234+2359 (right panel). All models are AMES-Dusty. See Tab. 1 for parameters.

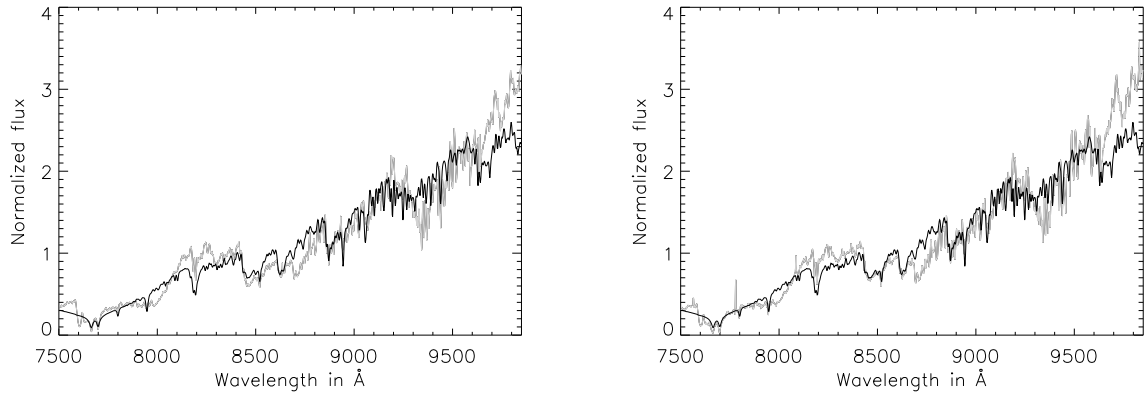


Fig. 2.— Fits (dark line) to the observed dwarfs (grey line) to 2M0345+2540 (left panel) and 2M0147+3453 (right panel). All models are AMES-Dusty. See Tab. 1 for parameters.

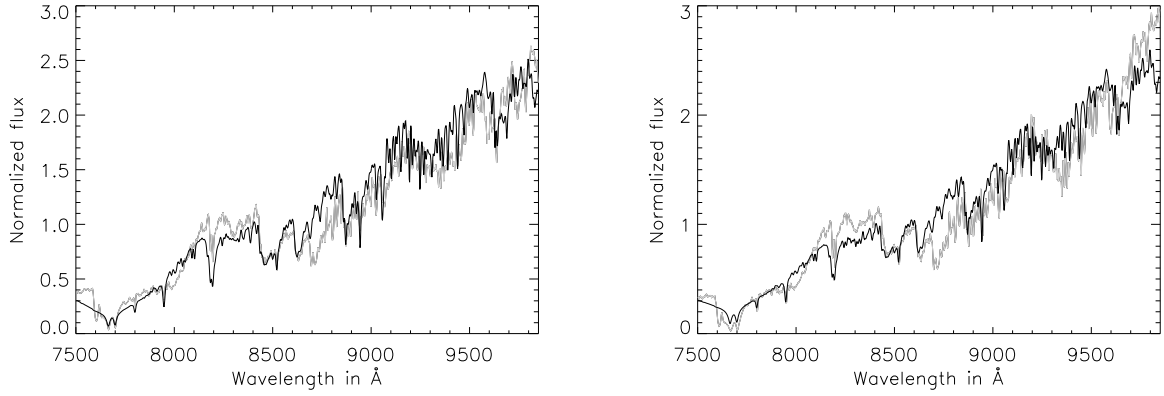


Fig. 3.— Fits (dark line) to the observed dwarfs (grey line) to 2M0746+200 (left panel) and 2M1439+1929 (right panel). All models are AMES-Dusty. See Tab. 1 for parameters.

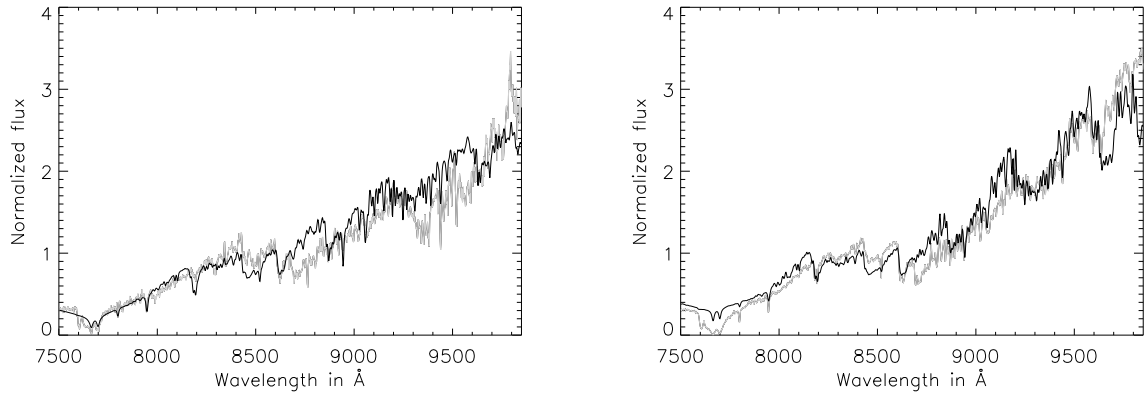
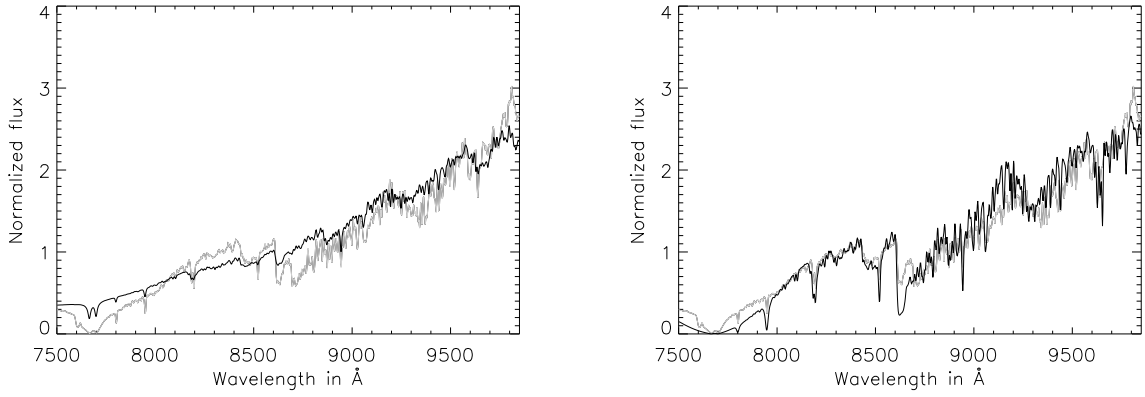


Fig. 4.— Fits (dark line) to the observed dwarfs (grey line) to 2M1726+1538 (left panel) and 2M1146+2230 (right panel). All models are AMES-Dusty. See Tab. 1 for parameters.



2M0036+1821

Fig. 5.— Fits (dark line) to the observed dwarfs (grey line) to 2M0036+1821. The model in the left panel is AMES-Dusty, the model in the right panel is AMES-Cond. See Tab. 1 for parameters.

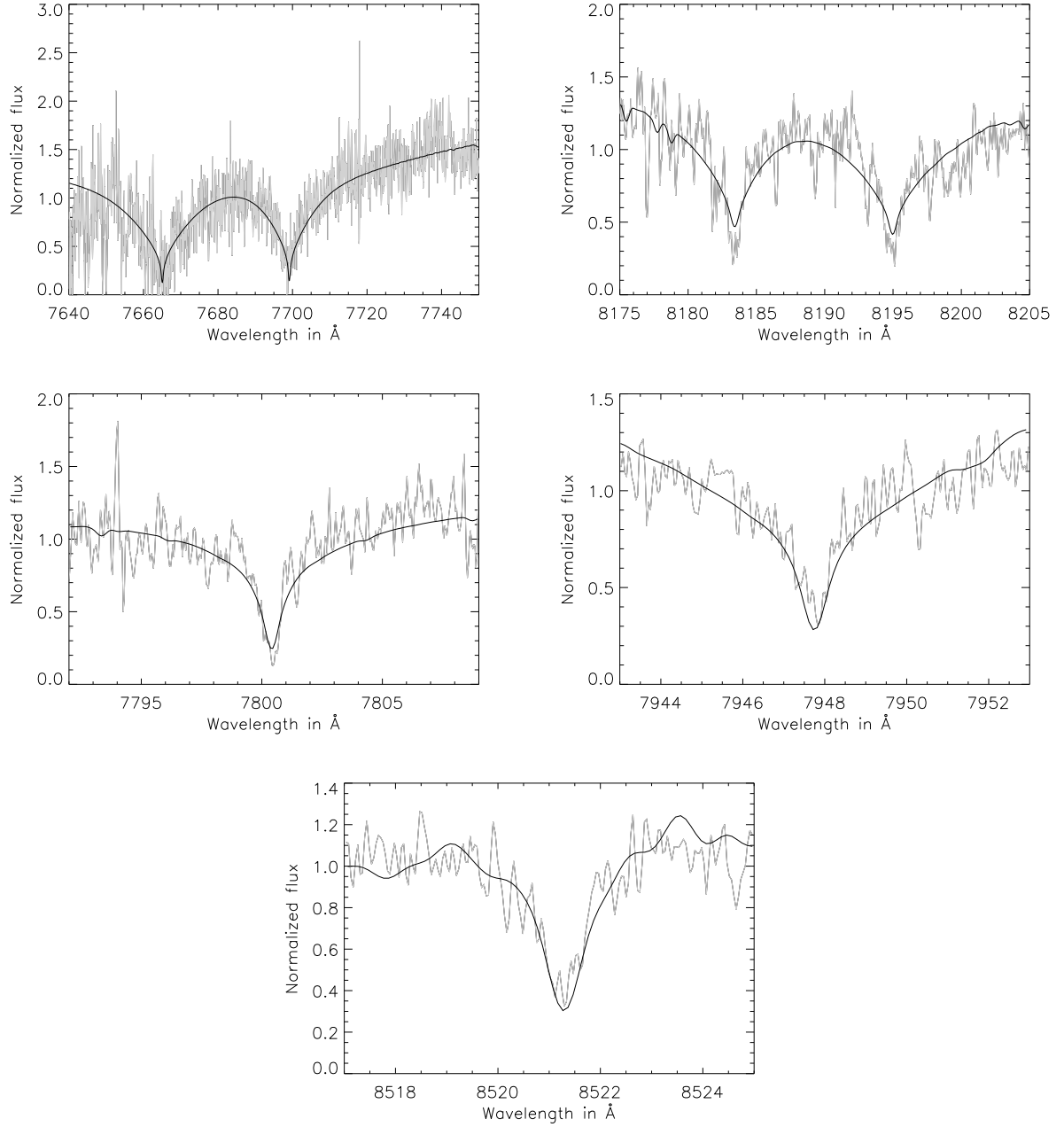


Fig. 6.— Fits (dark line) to 2M0149+2956 (grey line). See Tab. 2 for parameters. Telluric features have not been removed.



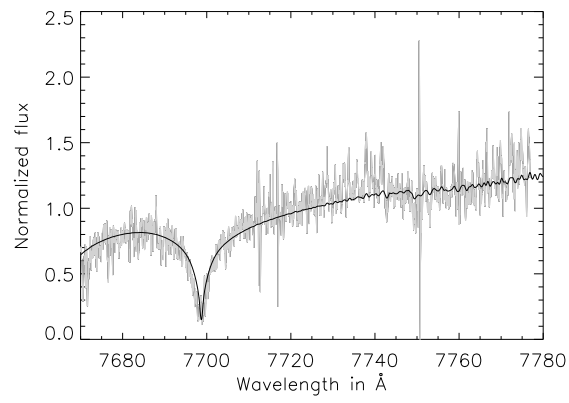


Fig. 7.— Fits (dark line) to 2M2234+2359 (grey line). See Tab. 2 for parameters. Telluric features have not been removed.

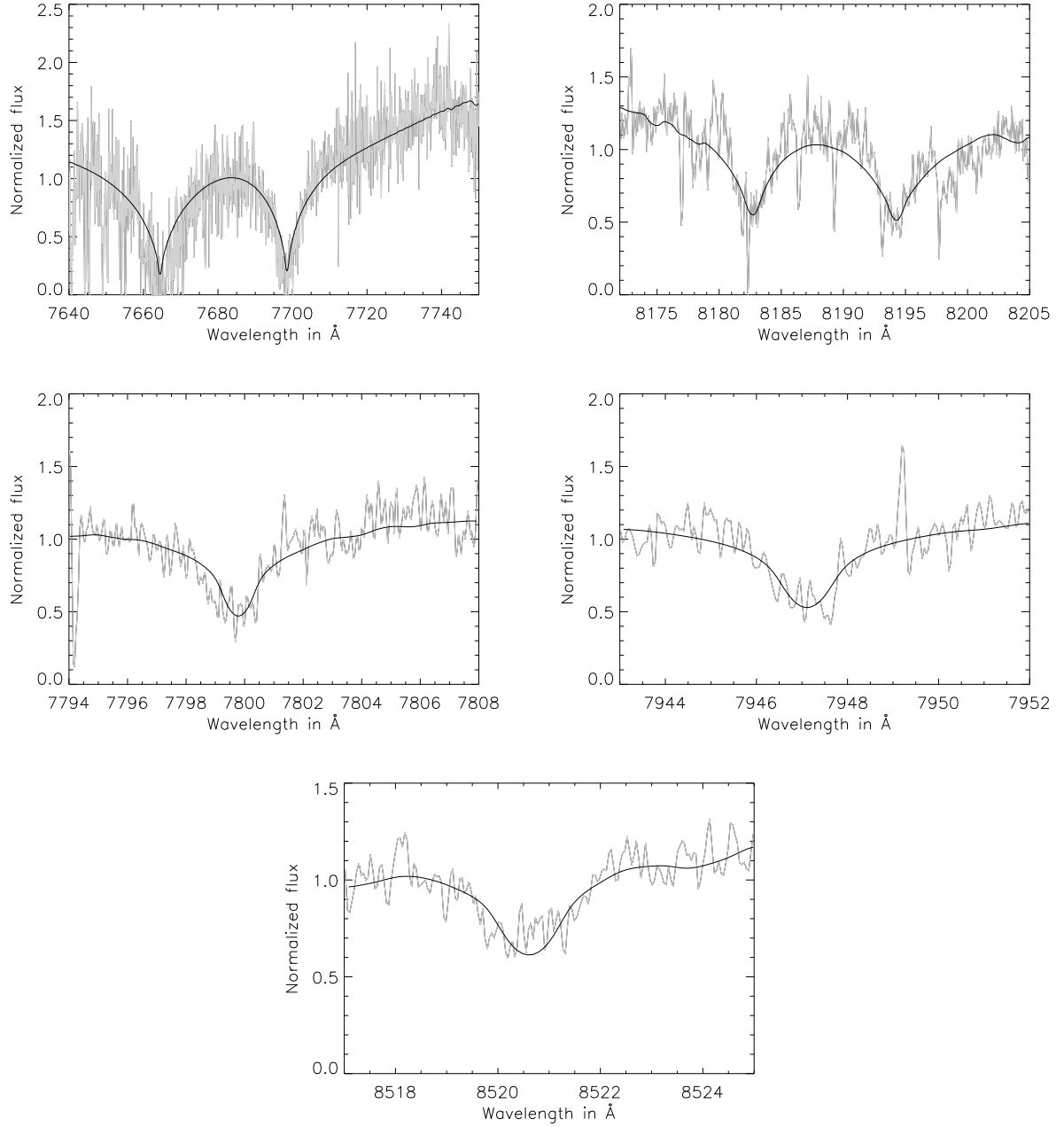


Fig. 8.— Fits (dark line) to 2M0345+2540 (grey line). See Tab. 2 for parameters. Telluric features have not been removed.

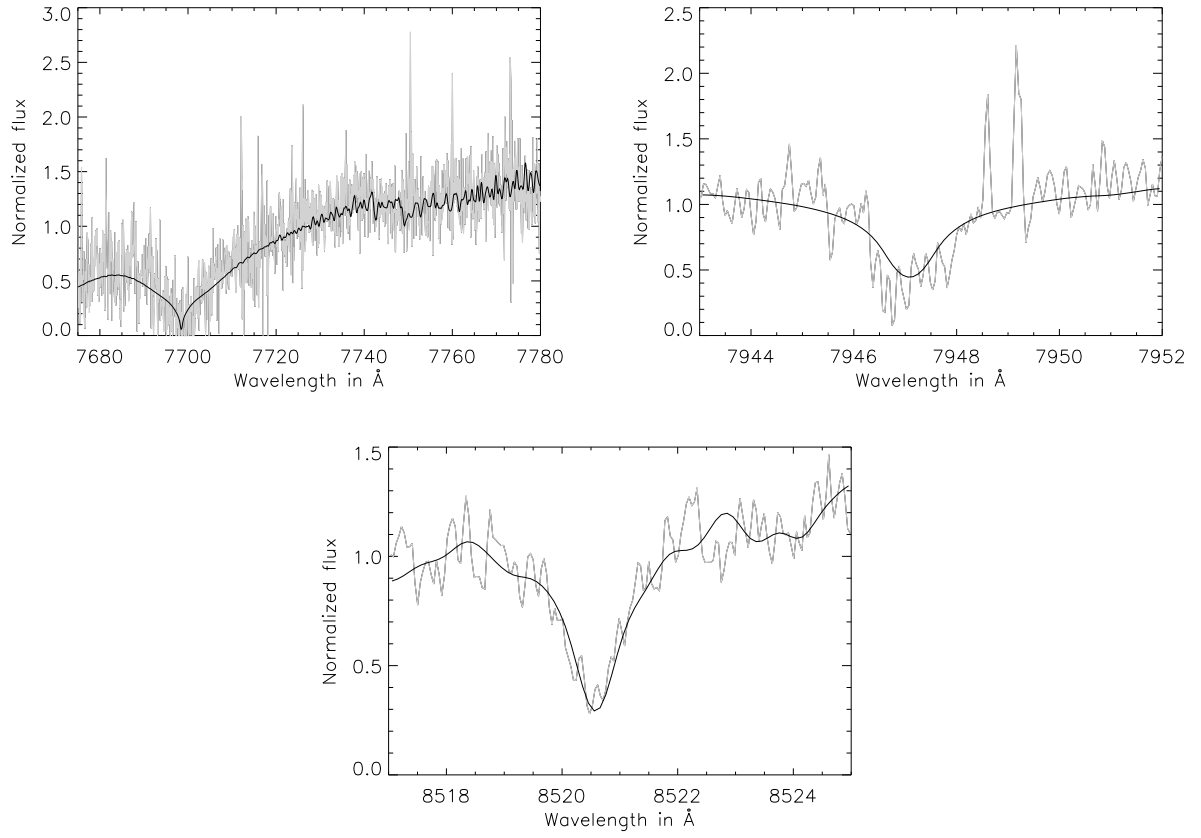


Fig. 9.— Fits (dark line) to 2M0147+3453 (grey line). See Tab. 2 for parameters. Telluric features have not been removed.

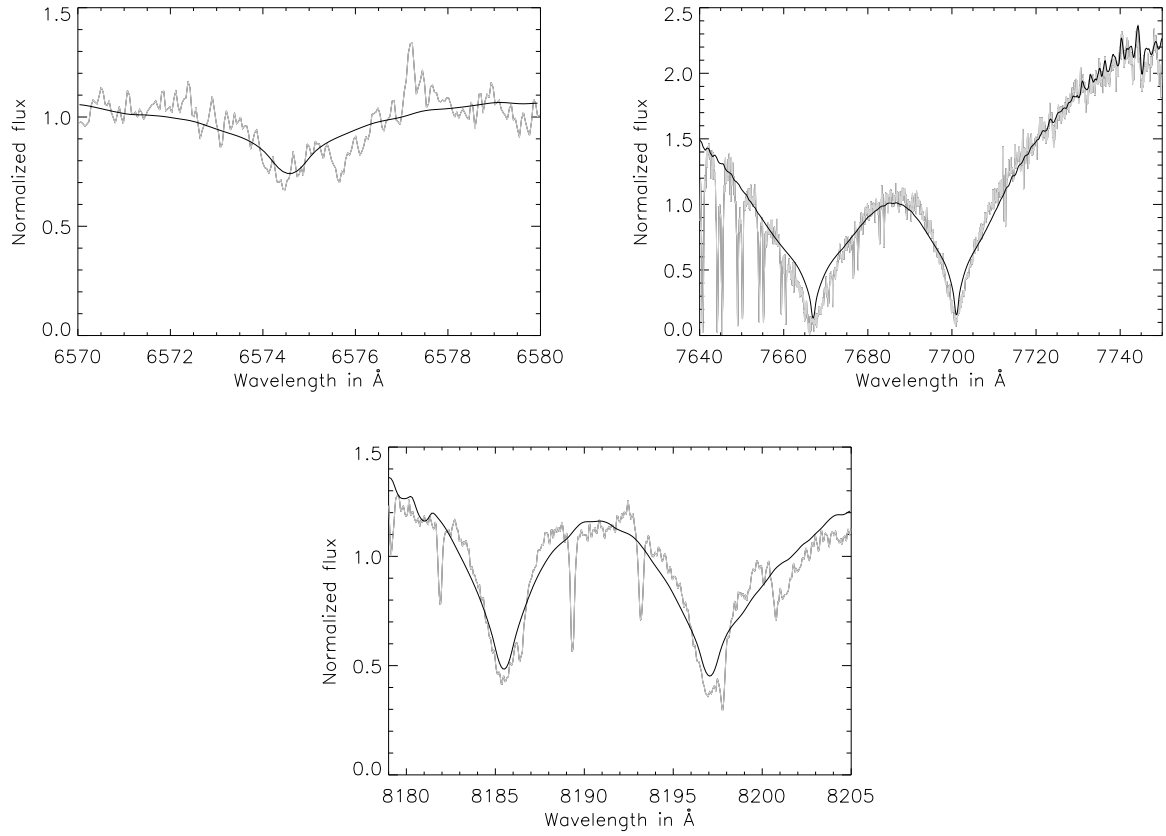


Fig. 10.— Fits (dark line) to 2M0746+200 (grey line). See Tab. 2 for parameters. Telluric features have not been removed.

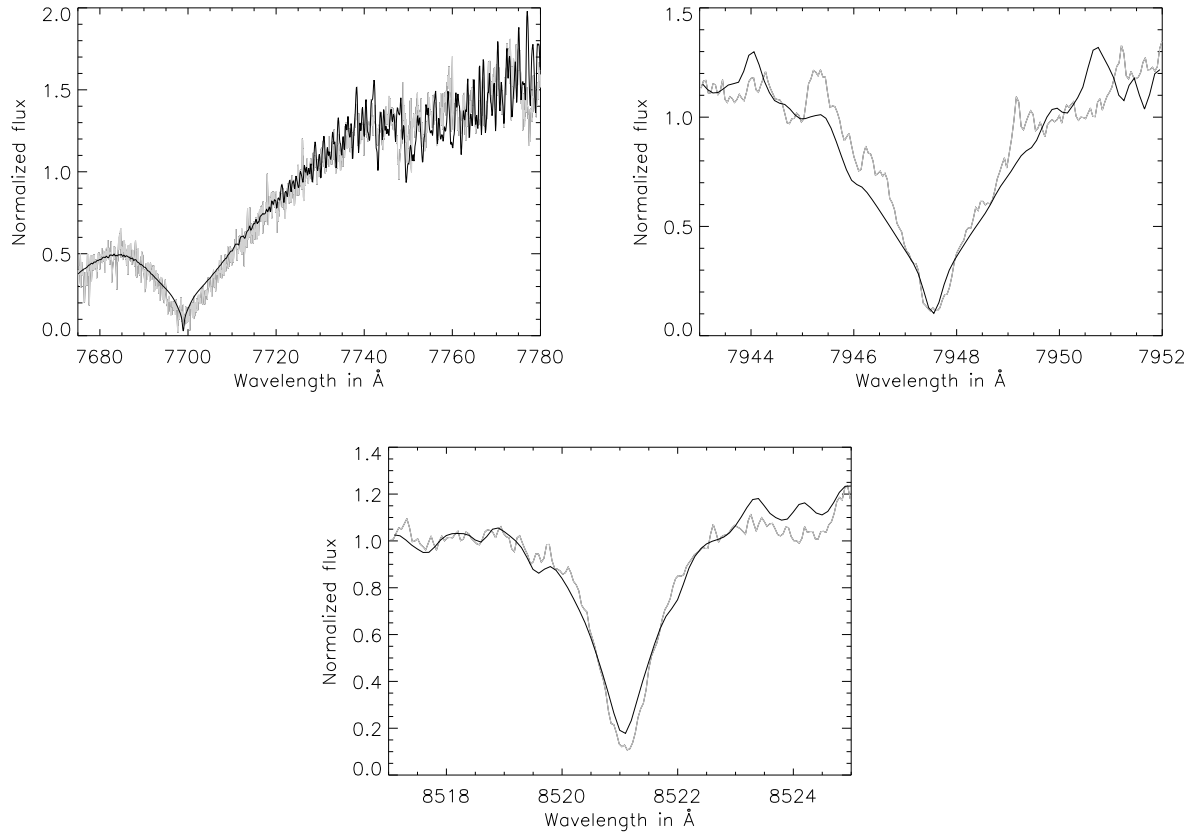


Fig. 11.— Fits (dark line) to 2M1439+1929 (grey line). See Tab. 2 for parameters. Telluric features have not been removed.

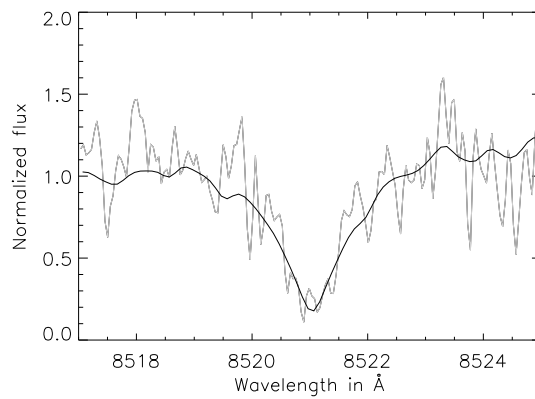


Fig. 12.— Fits (dark line) to 2M1726+1538 (grey line). See Tab. 2 for parameters. Telluric features have not been removed.

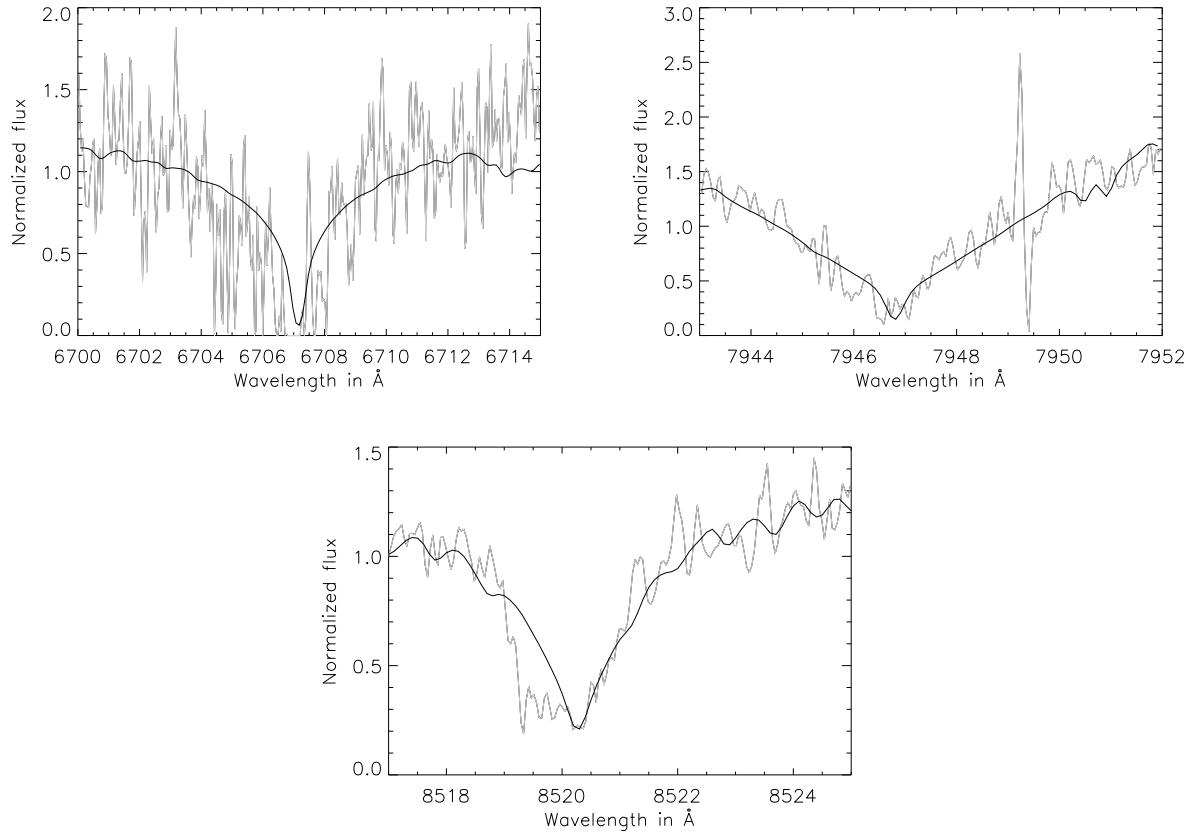


Fig. 13.— Fits (dark line) to 2M1146+2230 (grey line). See Tab. 2 for parameters. Telluric features have not been removed.

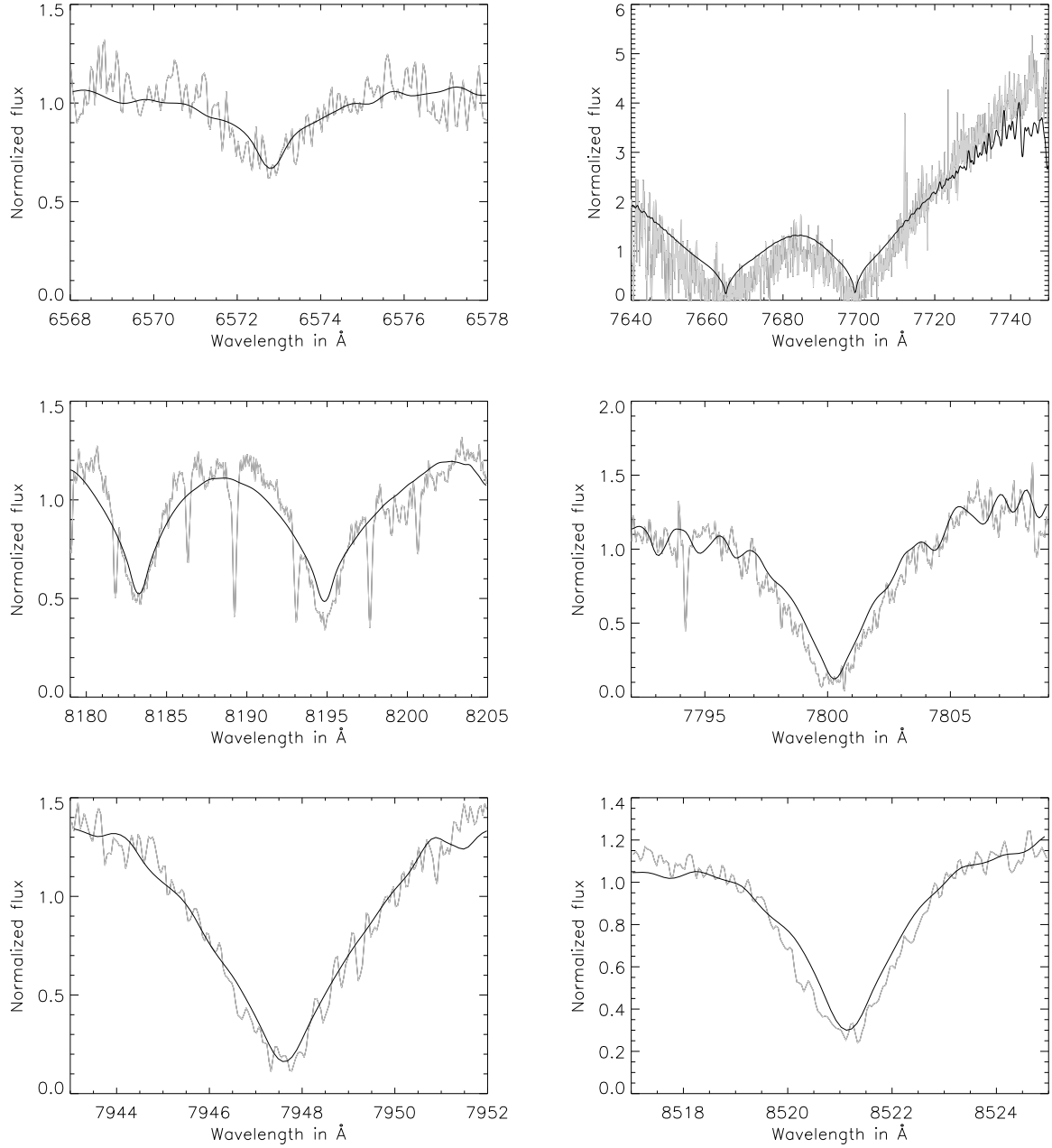


Fig. 14.— Fits (dark line) to 2M0036+1821 (grey line). See Tab. 2 for parameters. Telluric features have not been removed.

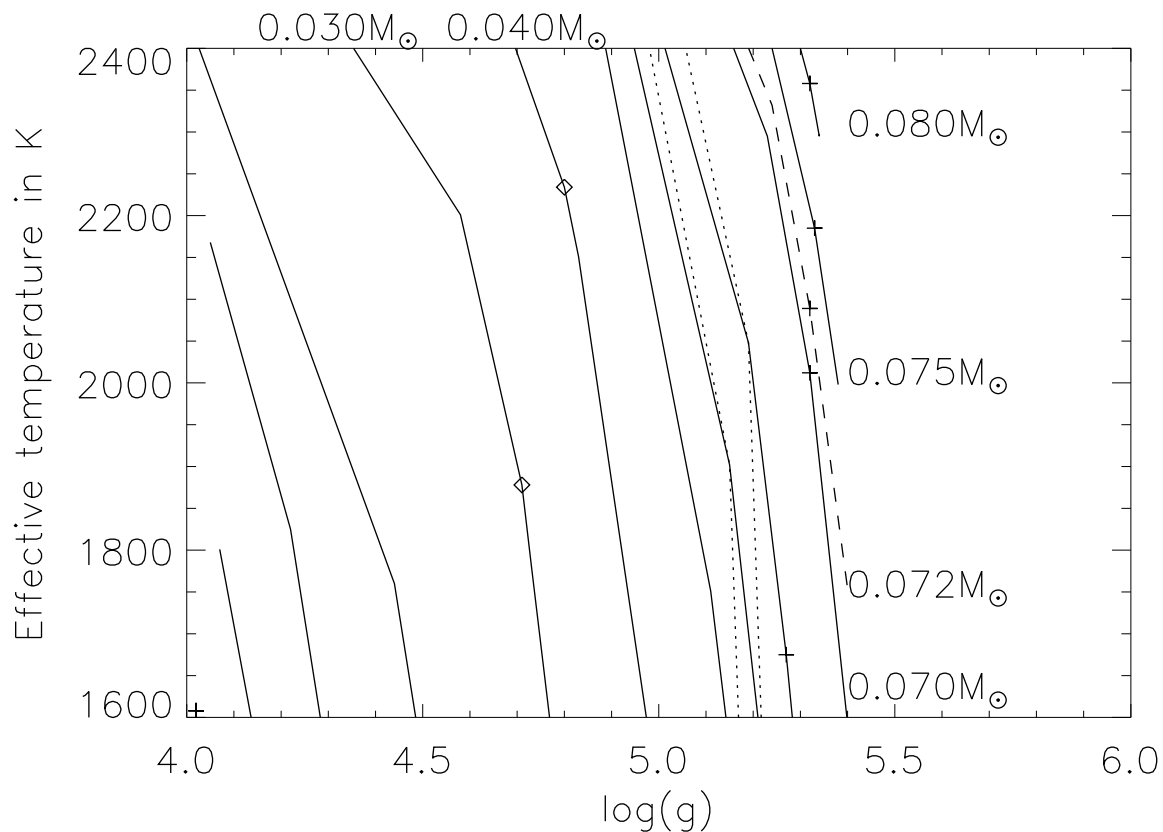


Fig. 15.—  $T_{\text{eff}}$  versus  $\log(g)$  from the data given by Chabrier et al. (2000). Each line represents the track for a certain mass. Some masses are indicated on the right and on the top. The dashed line is the minimum stellar mass. The dotted lines represent 95% Li abundance remaining (left line) and 50% Li abundance remaining (right line). The diamonds are the points where the objects are 100 Myrs old, the crosses where they are 1 Gyr old.



Table 1. Parameters from the low resolution fits for the objects in the sample.

Name	Spectral Type	AMES-Dusty		AMES-Cond	
		$T_{\text{eff}}$	$\log(g)$	$T_{\text{eff}}$	$\log(g)$
2M0149+2956	M9.5	2100	6.0	2100	6.0
2M2234+2359	M9.5	2000	6.0	2000	6.0
2M0345+2540	L0	1900	6.0	1800	5.5
2M0147+3453	L0.5	1900	6.0	1800	5.5
2M0746+200	L0.5	2000	6.0	2000	6.0
2M1439+1929	L1	1900	6.0	1800	5.5
2M1726+1538	L2	1900	6.0	1900	6.0
2M1146+2230	L3	1800	5.0	1800	5.5
2M0036+1821	L3.5	1800	5.5	1800	5.5

Table 2. Parameters from the high resolution fits for the objects in the sample.

Name	Spectral Type	K I 7685Å		Rb I 7800Å		Rb I 7948Å		Na I 8190Å		Cs I 8521Å		Ca I 5673Å		$v_{\text{rot}}$
		$T_{\text{eff}}$	$\log(g)$	$T_{\text{eff}}$	$\log(g)$	$T_{\text{eff}}$	$\log(g)$	$T_{\text{eff}}$	$\log(g)$	$T_{\text{eff}}$	$\log(g)$	$T_{\text{eff}}$	$\log(g)$	
2M0149+2956	M9.5	2000	6.0	2000	6.0	2000	6.0	2000	6.0	2000	5.0			10
2M2234+2359	M9.5	1900	5.0											15
2M0345+2540	L0	2100	6.0	1900	5.0	1800	6.0	1800	5.5	1900	5.5			25
2M0147+3453	L0.5	2000	5.0			1900	6.0			2000	5.0			10–20
2M0746+200	L0.5	2000	5.0					1900	5.0			1900	5.5	20
2M1439+1929	L1	2100	5.0			1900	4.5			2100	5.5			
2M1726+1538	L2									2100	5.5			
2M1146+2230	L3		$\geq 5.0$			2100	6.0			2000	5.5	2000 <sup>a</sup>	5.5 <sup>a</sup>	
2M0036+1821	L3.5	2100	5.0	2100	5.0	2000	5.0	1900	5.5	2100	6.0	1800	5.0	15

<sup>a</sup>These are from the Li I 6708Å line.